Journal of Molecular Liquids 399 (2024) 124480

Contents lists available at ScienceDirect

Journal of Molecular Liquids

journal homepage: www.elsevier.com/locate/molliq

Silver nanoparticles modified titanium carbide MXene composite for RSM-CCD optimised chloride removal from water

Roya Moosaei [a], Samad Sabbaghi [a,b,*], Mohammad Sadegh Jafari Zadegan [a], Kamal Rasouli [c], Samaneh Ghaedi [d], Hamid Rajabi [e,*]

[a] Department of Nano-Chemical Engineering, Faculty of Advanced Technologies, Shiraz University, Shiraz, Iran
[b] Nanotechnology Research Institute, Shiraz University, Shiraz, Iran
[c] Department of Chemical Engineering, School of Chemical and Petroleum Engineering, Shiraz University, Shiraz, Iran
[d] School of Engineering, the University of Manchester, Manchester M13 9PL, UK
[e] Department of Civil and Environmental Engineering, School of Engineering, University of Liverpool, Liverpool L69 3GH, UK

ARTICLE INFO

Keywords:
MXene
Adsorption
Chloride ion
Drinking water
Environmental remediation

ABSTRACT

Unsafe levels of chloride in drinking water can make it unpalatable, susceptible to infrastructure corrosion and prone to heavy metals mobility. Conventional chloride mitigation strategies are subjected to inefficient performance and costly operation, necessitating innovations for more sustainable, affordable, and scalable technologies. In this study, silver nanoparticles-modified Ti_3C_2 MXene nanocomposite (AgMX) is synthesised via dry impregnation method for effective removal of chloride ion from water. The composite physicochemical properties were thoroughly characterised using various analytical techniques, including TEM, SEM, XRD, EDS, BET, zeta potential and pH_{pzc} analysis. The experimental testing was optimised using CCD-RSM method in terms of adsorbent dosage (0.2–2 g/L), reaction time (1–17 min), and chloride concentration (10–90 mg/L). Under optimal conditions (adsorbent:1.55 g/L, time: 12.19 min, & concentration: 52.17 mg/L), a promising chloride removal of 91.8 % was achieved. Langmuir model showed the best fit to adsorption isotherm (R^2: 0.9852) comparing to Freundlich and Dubinin-Kaganer-Radushkevich (DKR) isotherms, while pseudo-second-order kinetic model offered the closest data to the experimental results (R^2: 9893) compared to the pseudo-first-order, Elovich and Intraparticle diffusion models R^2: 0.2335,0.1212 and 0.2050, respectively. The composite reusability and regeneration potential after four repeated cycles were found practically efficient as $\geq$ 68 % and $\geq$ 84 %, respectively. The outcomes of this study can demonstrate the efficiency of the formulated composite as a promising material for the sustainable treatment of chloride-contaminated water.

1. Introduction

Ensuring inclusive and widespread access to safe water is an imperative goal to promote public health and sustainable development, particularly impacting vulnerable populations and marginalised individuals [1–4]. Safe water accessibility is now under stress by climate change, industrialisation, urbanisation, population growth and environmental pollution [5–7]. Saline water, also known as saltwater, is a global issue with significant implications for global health, clean water accessibility, agricultural sustainability, ecosystem balance, infrastructure health, and economy [8–11]. Effective water management, desalination, soil improvement, sustainable agriculture, and environmental conservation are key solutions to prevent unsafe levels of salinity in water [12–15]. Despite the truth that there are various contaminants such as dyes, heavy metals, and pollutants that also demand attention, the selection of chloride as the target pollutant for adsorption in the research holds importance due to its prevalence and adverse consequences. Moreover, chloride ions are a significant type of the dissolved salts, along with sodium, magnesium, and calcium, contributing to the salinity of waterways. The importance of removing chloride ion from water lies in its potential to cause harm to both human and other living species health and the environment. Chloride ion, as a mineral compound, can have detrimental effects on the quality of water and the ecosystems it supports. Chloride is naturally present in water bodies mainly due to mineral dissolution in the Earth's crust (salt deposits in rocks and soils) in addition to a range of anthropogenic sources such as

* Corresponding author at: Department of Civil and Environmental Engineering, School of Engineering, University of Liverpool, Liverpool L69 3GH, UK.
E-mail addresses: sabbaghi@shirazu.ac.ir (S. Sabbaghi), hamid.rajabi@liverpool.ac.uk (H. Rajabi).

https://doi.org/10.1016/j.molliq.2024.124480
Received 1 January 2024; Received in revised form 10 March 2024; Accepted 12 March 2024
Available online 14 March 2024

industrial processes, road salt application, wastewater discharge, agricultural runoff, and domestic activities [16,17]. High levels of chloride can be disruptive to water ionic balance affecting the health of aquatic ecosystems, massively corrosive to infrastructure (bridges, pipelines, and water distribution systems), and origins of unpleasant taste and odour which necessitates the need for effective chloride control methods for safe and palatable drinking water [18].

The conventional water desalination methods are reverse osmosis (RO), forward osmosis (FO), multi-stage flash (MSF) distillation, multi-effect distillation (MED) and electrodialysis (ED). RO as a promising energy-efficient approach which Effectively removes chloride ions and other contaminants is energy-efficient compared to thermal desalination methods and suitable for treating high salinity water sources. While it suffers from high operational costs, require of pre-treatment to prevent membrane fouling and producing concentrated brine waste that needs proper disposal [19]. FO is an appealing energy-efficient and environmentally friendly with low energy consumption, uses low-grade heat sources for operation and is less prone to fouling compared to RO [20]. MSF, likewise offers some advantages like capability of handling high seawater salinity levels, being a matured technology with high reliability and can be cost-effective for large-scale operations. Though, it also has limitations like energy-intensive due to heating seawater, prone to scaling and corrosion issues and high capital costs [21]. MED, since is more energy-efficient compared to MSF, can produce high-quality water and be integrated with renewable energy sources. Although, besides high capital costs, it requires careful maintenance to prevent scaling and corrosion and is limited to certain feedwater qualities [22]. ED is energy-efficient compared to thermal methods, can operate continuously and be effective for treating brackish water, but it still is not widely used due to being limited to low to medium salinity water, membrane fouling can occur, furthermore it requires electricity for operation which raises the costs. As explained shortly, each desalination method has its unique advantages and disadvantages, and the choice of technique depends on factors such as water source characteristics, energy availability, operating costs, and environmental considerations.

Adsorption techniques have been used in industrial wastewater treatment and possess many advantages, such as high efficiency, low operational cost, and more environmentally friendly if compared with conventional treatment strategies, and aims to reduce components such as toxic components, that hard to apart, multivalent heavy metal ions like Cu^{2+}, Pb^{2+} or synthetic dyes, implementing different low-cost adsorbents, even like algae, bagasse, activated carbons or other potential materials [23–30]. Chemical desalting as one of adsorption methods, fuelled recently by innovations in nanomaterials synthesis, have emerged as a promising technique in removal of inorganic and organic pollutants, such as particularly chloride ions from water, which can be used independently or in conjunction with other processes to enhance desalination efficiency. MXene is an emerging type of two-dimensional materials composed of transition metal carbides, nitrides, or carbonitrides, with remarkable hydrophilicity, high electronic conductivity, and feasible scalability. It has a tuneable interlayer spacing, adaptable surface chemistry, and porous structure, making its application suitable in composite materials for environmental protection in capturing a wide range of pollutants such as Cr^{6+} [31], Cr^{3+}, Hg^{2+} [32], urea, Pb^{2+}, Cu^{2+} [33], and strontium ions [34]. Using AgNPs-modified Ti_3C_2 MXene nanocomposite (AgMX) for the adsorption of chloride offers several advantages that make it a promising material for this purpose. AgMX has a high surface area due to its nanocomposite structure, which provides ample active sites for chloride adsorption. The combination of AgNPs and Ti_3C_2 MXene enhances the adsorption capacity of the material, making it more efficient in removing chloride ions from solution. AgMX has shown selectivity towards chloride ions which is crucial in applications where targeted removal of chloride is required without affecting other components in the solution. Silver nanoparticles (AgNPs) exhibit antibacterial properties, which can be beneficial in applications where inhibiting bacterial growth is important and can help in preventing microbial contamination during the adsorption process[35–37]. Ti_3C_2 MXene is known for its robustness and stability, which can contribute to the durability of the adsorption material. The AgNPs modification can further enhance the stability of the nanocomposite. Additionally, AgMX can be regenerated and reused multiple times, making it a cost-effective option for chloride removal compared to some other materials. The use of MXene, which is derived from abundant natural sources, coupled with the recyclability of the material, makes it an environmentally friendly choice for water treatment applications. Despite the promising characteristics of AgMX, it is essential to continue research and development on other materials for adsorption applications to explore their potential benefits and address specific challenges. On the other hand, among different methods of optimising experiments, Response Surface Method (RSM) based Central Composite Design (CCD) as a statistical and mathematical approach to simultaneously optimize multiple parameters in reactions, instead of routine optimization which examines one parameter while keeping the others constant, is a laborious task and fails to include the combined impacts of different parameters on the adsorption [1,24,38,39]. Furthermore, In the case of adsorption experiments, CCD allows for the exploration of both linear and quadratic effects of factors, as well as the investigation of potential interactions between variables. Though, other RSM models such as full factorial and Box-Behnken design have their own advantages and limitations. Full factorial designs can be resource-intensive when dealing with multiple factors at various levels, while Box-Behnken designs may not efficiently capture the curvature in the response surface as effectively as CCD [40]. The selection of CCD over other RSM models is often driven by the need to efficiently explore the experimental space, identify optimal conditions, and understand the interplay between various factors in the adsorption process. Consequently, the mentioned combination was chosen as an affordable, feasible and inclusive method using Design of Experiment (DOE) software to efficiently model complex processes and optimize multiple variables the adsorbent dosage, chloride concentration, and contact time [41].

In the context of the discussed subjects, this study addresses the following novelties:

- The Ti_3C_2 MXene was prepared via etching of Al from the Ti_3AlC_2 MAX phase.
- The binary-adsorbent was synthesized through the self-reduction of Ag^+ ions to silver nanoparticles on the surface of Ti_3C_2, resulting in the formation of AgMX composite. This process utilized dry impregnation, known for its cost-effectiveness and ease of implementation.
- Utilizing a minimal quantity of silver nanoparticles, the surface modification of Ti_3C_2 MXene led to a significant increase in adsorption capacity, thereby reducing the inherent usage of MXene, which possesses intrinsic adsorption capabilities.
- The characterization of the adsorbent was conducted using various analytical techniques, including XRD, BET, TEM, SEM, EDS analyses Zeta potential measurements, pH of zero-point charge (pH_{pzc}).
- The investigation into the underlying adsorption mechanisms was carried out through the utilization of different isotherms. Subsequently, the kinetics of chloride removal were examined, leading to the proposal of a mechanism for chloride adsorption.
- To the best of our knowledge, this study represents the pioneering research endeavor focusing on a Ti_3C_2 MXene-based adsorbent for the efficient adsorption of chloride ions from potable water sources.
- The optimization of operational parameters in the chloride ion removal process was carried out using the RSM-CCD approach.

2. Materials and methods

2.1. Materials

Titanium Aluminium Carbide with a composition of Ti_3AlC_2 (99 %)

was obtained from American Element Co. (USA), and silver nitrate ($AgNO_3$, 99 %) was acquired from Merck. The etchant solution consisted of Hydrofluoric Acid (HF, 40 %) was purchased from Sigma Aldrich, and deionized water (DW) was procured from Aseman Co. (Iran). All chemicals were used as received without any further modification/ purification.

2.2. $Ti_3C_2T_x$ Mxene synthesis

The synthesis of Ti_3C_2 MXene involved the etching of Ti_3AlC_2 MAX phase precursor using hydrofluoric acid solution. Initially, 1 g of Ti_3AlC_2 was slowly added to a beaker containing 25 ml of HF 40 % solution (Fig. 1a). The gradual addition of MAX phase was necessary to prevent excessive bubbling, typically taking 5 to 10 min. The resulting dispersion was then stirred for 8 h with a moderate rotation speed (300 rpm) and at room temperature. The obtained black slurry was thoroughly rinsed with DW and then centrifuged at 3500 rpm for 5 min until a neutral pH was achieved. The supernatant was then discarded, and the sediment was vacuum-dried under N_2 for 6 h at the ambient condition to obtain the desired multi-layered Ti_3C_2 black powder stored for further modifications and testing.

2.3. AgMX nanocomposite synthesis

The AgMX nanocomposite was synthesised via dry impregnation method (Fig. 1b). A solution was first prepared by adding 0.12 g of silver nitrate to 10 ml of DW. The solution was stirred (200 rpm, 10 min), sonicated for 2 min at 100 W, and gradually added into a vial containing 0.04 g of Ti_3C_2 to ensure a full coating of all MXene surfaces. The sample was then oven-dried at 90 °C for 2 h to be modified under heating. The thermally treated materials were then submerged in DW (10 ml), sonicated for 2 min and stirred (200 rpm, 10 min, room temperature) for 10 min to make sure of complete removal of all excess and unreacted nitrate compounds. The resulting mass was then allowed to rest for 30 min, and once the upper solution overflowed, the AgMX was subjected to oven drying at 50 °C for 3 h.

2.4. Characterisation techniques

Various analytical methods were employed to characterise the synthesised materials in terms of crystallinity, morphology, elemental composition, silver nanoparticle impregnation, porosity, and surface charge. X-ray powder diffraction (XRD) was conducted (Paralytical

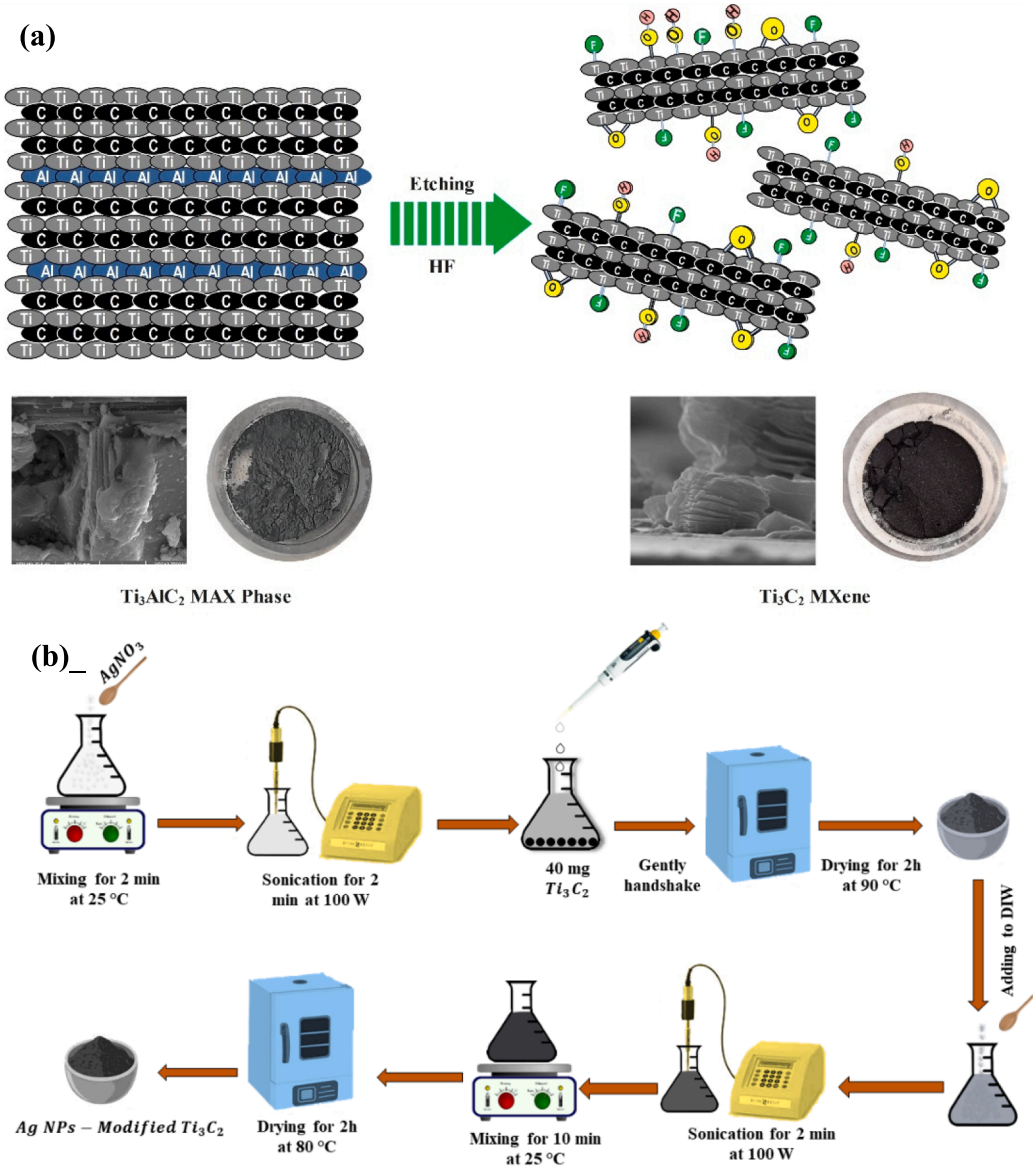

Fig. 1. Schematic of a) Multi-layered Ti_3C_2 with different termination groups (-F, -OH and -O) and b) AgMX synthesis.

X'pert Pro, Netherlands) over a 2θ range of 5-80° to assess Ti_3C_2 crystallinity and morphology. Scanning electron microscopy (SEM) combined with energy-dispersive X-ray spectroscopy (EDS) and elemental mapping was carried out (TESCAN-Vega 3, Czech) to analyse surface morphology and elemental composition. Impregnation of silver nanoparticles in Ti_3C_2 was evaluated via transmission electron microscopy (TEM) (Philips 208 s, Netherlands). The Micromeritics ASAP 2010 (Japan) at 350℃ with N_2 was used to investigate materials porosity based on Brunauer-Emmett-Teller analysis (BET) method. Zeta potential of Ti_3C_2 and AgMX in aqueous solution and saline water, and pH of zero-point charge of AgMX were assessed (HORIBA Scientific SZ-100 Japan) to analyse materials surface charge and stability.

2.5. Chloride removal testing

The predetermined quantities of AgMX adsorbent, based on the Design of Experiments (DOE) outcomes (see Section 3.4), were added to a 15 ml solution of chloride ions, stirred for a specific contact time under ambient conditions, centrifugated five times at 7000 rpm for 7 min, of which the supernatant was collected for further analysis. The removal of chloride ion was calculated using Eq. (1).[23]

$$Chlorideionremoval(\%) = \frac{c_0 - c_t}{c_0} \times 100 \quad (1)$$

where, C_0 and C_t are the initial and final concentration of chloride ion at time t, respectively.

2.6. Design of experiments

The Design Expert software was used as valuable and practical tool to examine three key variables of adsorbent dose, time and initial chloride concentration significantly affecting the efficiency of chloride ion removal by the synthesised AgMX adsorbent. Response Surface Methodology (RSM) was also employed to optimise the operational parameters and responses, while reducing the number of required experiments. Within the realm of RSM approaches, the central composite design (CCD) method was found to be highly effective and promising which involved crafting a second-order response surface model with five levels (-2, −1, 0, 1, 2) for individual variables. The distance between each level and the value of α quantified the separation between the centre and axis points of the experimental design. Table S1 outlines the significant factors and their respective levels that were integral in removing chloride ions using AgMX. It should be noted that the range of influential parameters was determined based on reported values and preliminary tests.

3. Results and discussion

3.1. XRD and SEM/EDS analysis

The crystal structure and synthesis quality progression from MAX Phase to MXene are assessed via X-ray Diffraction analysis as shown in Fig. 2, revealing key diffraction peaks of the MAX phase at angles of 39° (corresponding to the (1 0 4) plane) and 9.5° (corresponding to the (0 0 2) plane). These peaks signify the presence of aluminium layers and the interlayer spacing, respectively. Additional peaks at 2θ angles of 18.9°, 33.9°, 7.36°, 8.38°, 7.41°, 3.48°, and 25.60° are identified, aligning with planes (0 0 4), (1 0 1), (1 0 3), (1 0 4), (1 0 5), (1 0 7), and (1 1 0) as per the Powder Diffraction File (PDF) 52–0875 [42,43]. The XRD pattern also confirms the absence of impurities in the MAX phase, particularly Ti_2AlC [44]. Moreover, after the etching process, the peak at 2θ = 39 Â° corresponding to (1 0 4) plane, the atomic layer of Al in structure of Ti_3AlC_2, completely disappeared, expressing the complete etching of this element by HF from MAX phase proving proper synthesis of Ti_3C_2. It also should be noted that the other (00*L*) peaks, related to

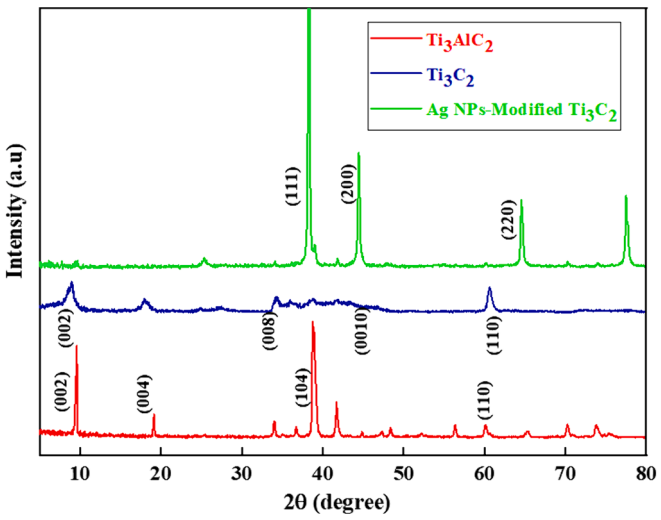

Fig. 2. XRD spectra of Ti_3AlC_2, Ti_3C_2 and AgMX.

base plate of two-dimensional layers of titanium carbide, shifted to lower Bragg angles – particularly for (0 0 2) which shifted from 9.5 Â° to 8.8 Â° [45]. This shift in the peak position can be attributed to the widening of the interlayer spacing, a consequence of the replacement of aluminium atomic layers with O, OH, and F functional groups (dependent on the etchant used), as well as the final integration of water and ions. Three distinct diffraction peaks are evident in Fig. 2, depicting silver nanoparticles. The most significant peak, found at a 38 Â°, holds high intensity associated with the (1 1 1) plane, indicative of the cubic crystalline structure of silver (J CPPS, NO. 04–0783). The presence of well-crystallised silver nanoparticles within the composite is illustrated by this peak, and its intensity is contingent upon the quantity and ratio of silver nanoparticles to Ti_3C_2 [46]. Peaks observed at 44 Â° and 64 Â° align with (2 0 0) and (2 2 0) planes, respectively, affirming the existence of single crystal silver and substantiating the formation of silver nanoparticles. The intensity of the (0 0 2) peak, a primary characteristic of Ti_3C_2, diminishes with the inclusion of silver nanoparticles [35]. SEM and TEM analysis as follow provide a comprehensive view of the silver nanoparticle morphology and microstructure within the hybrid system, offering an enhanced resolution [46].

In Fig. 3, SEM images are presented alongside EDS spectra, illustrating both the MAX phase and Ti_3C_2, thus elucidating the etching process and identifying constituent chemical elements. The structural makeup of Ti_3AlC_2 is depicted in Fig. 3a, revealing its layered and tightly compressed configuration of titanium, aluminium, and carbide. The etching process is driven by the weak bond between titanium and aluminium elements. After etching, the interlayer spacing increases, resulting in thinner layers with evident smoothness (Fig. 3b), leading to the accordion-like expanded structure often observed in SEM images [44]. EDS analysis confirms the presence of titanium, oxygen, carbon, and fluorine elements within Ti_3C_2. Notably, the absence of aluminium in conjunction with the presence of fluorine validates the successful etching [42,47]. The composition of Ti_3AlC_2 is reported as 60.08 % titanium, 20.29 % aluminium, and 19.64 % carbon. The composition table for AgMX reveals that the adsorbent contains 50 % silver nanoparticles. Fig. 3 presents an elemental mapping image which depicts the adsorbent modified with silver nanoparticles. These images serve as means to assess the even distribution of various elements within the adsorbent [43]. In Fig. 3, a distinct pattern emerges, highlighting the elements of silver, oxygen, and titanium as the predominant constituents. Conversely, the presence of fluorine is minimal, aligning precisely with the information found in the EDS tables.

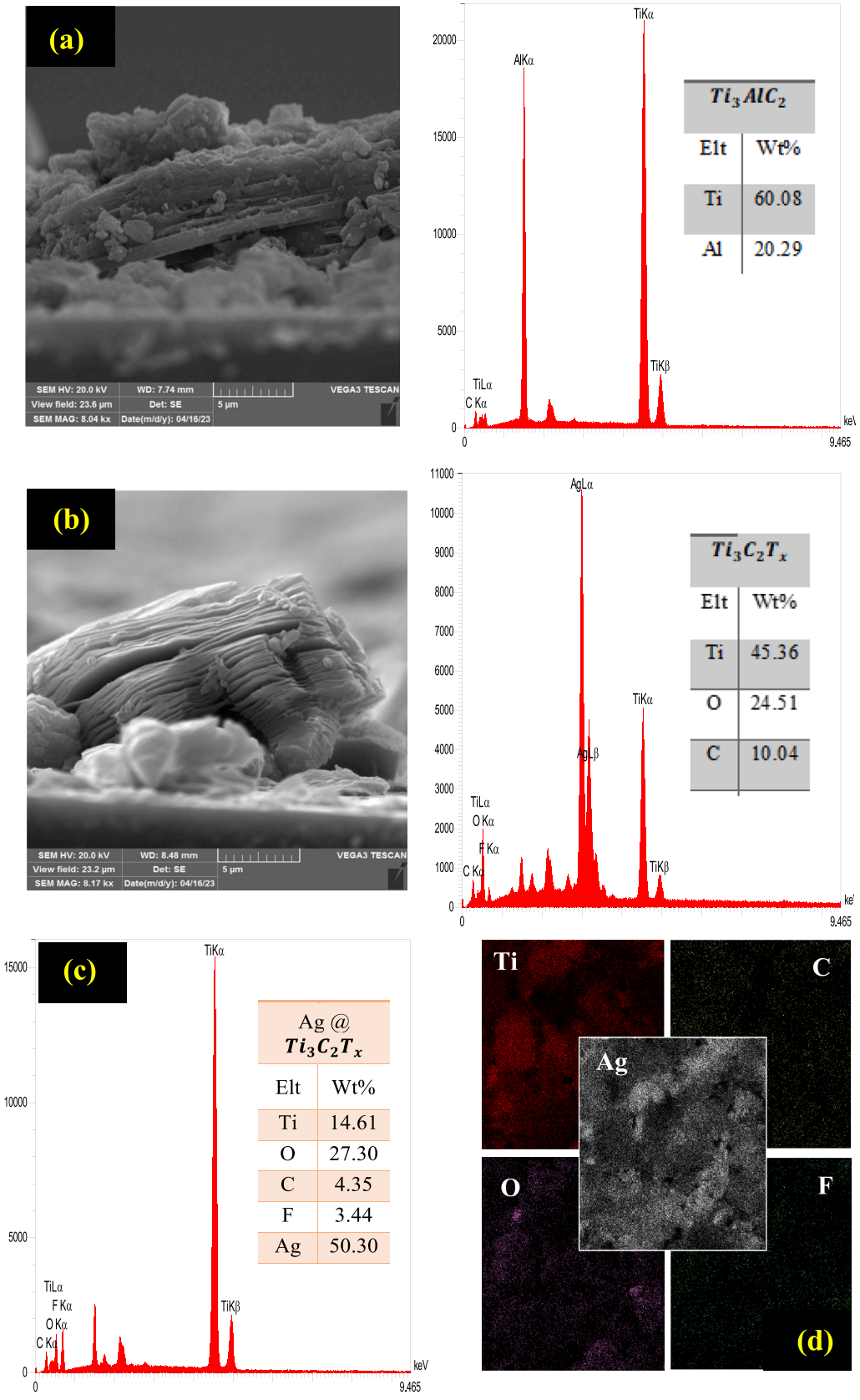

Fig. 3. SEM images and EDX spectra of (a) Ti_3AlC_2 and (b) Ti_3C_2, EDS spectra of c) AgMX and d) elemental mapping of Ti, O, C, F, Ag, respectively.

3.2. TEM, zeta potential and pH of zero-point charge analysis (pH_{pzc})

Transmission Electron Microscopy was used to examine the structure of as-synthesised silver nanoparticles on Ti_3C_2 complemented by Energy Dispersive X-ray (EDX) mapping and spectroscopy (EDS) for composition verification in the same regions observed by TEM (Fig. 3). TEM micrographs as shown in Fig. 4a revealed the distribution of Ag NPs on Ti_3C_2 flakes. These micrographs showed direct attachment of silver nanoparticles to Ti_3C_2, resulted in spherical features on the previously smooth Ti_3C_2 surface. Effective dispersion of silver nanoparticles on Ti_3C_2 occurred due to electrostatic repulsion which prevents agglomeration [46,48]. The size and shape of NPs varied due to rapid reduction of Ag^+ ions, making its control a challenge even with low concentrations of $AgNO_3$ solution. This led to diverse NP shapes like small/large spheres and semi-rectangular forms [35].

Zeta potential analysis is a crucial technique for assessing the stability of colloidal suspensions. It also aids in discerning the adsorbent surface charge, thereby offering valuable understanding of the electrostatic potential at the particle's surface. This factor plays a pivotal role in influencing the overall suspension stability. The zeta potential values of both Ti_3C_2 and AgMX synthesized in DW with varying NaCl concentrations are outlined in Fig. 4b. The zeta potential value of Ti_3C_2 in DW was −42.02 as frequently reported to be negatively charged [49], falling in the range of −30 to −80 which is contingent on the pH of the solution and the proportional composition of Ti_3C_2. The negative zeta potential of Ti_3C_2 significantly contributes to the colloidal solutions' stability, facilitating favourable dispersion within neutral solutions [42,49]. The zeta potential value for the Ti_3C_2 adsorbent, subsequently modified with silver nanoparticles, is detailed in Fig. 4b. Notably, the relevant literature affirm that silver nanoparticles exhibit a positive zeta potential, around 26.23. This positivity emanates from the presence of the CTAB capping agent. The shift in zeta potential shows that Ti_3C_2 is well integrated with silver nanoparticles, which is consistent with SEM and TEM findings [50].

The zeta potential of AgMX was also evaluated in 10, 50 and 90 ppm NaCl solution to measure the performance of the AgMX in different amounts of univalent electrolyte solutions. As provided in Fig. 4b, the negative values decrease with the increase in the concentration of the solution as an electrolyte solution, or in other words, it becomes more positive, which is due to the compression of the electric double layer in the presence of the electrolyte. Given the persistence of a negative surface charge despite the concentration increment, it is evident that the reversal of surface charge has not been brought about solely by the rising concentration, attributed to the augmentation of dissimilar charges encircling the electric double layer, causing a heightened compression of these dual layers [51].

To investigate the pH range where the surface of the adsorbent transitions from being negatively charged to positively charged, pH of zero-point charge (pH_{pzc}) was determined. This transition can affect the electrostatic interactions and the adsorption capacity of the material for chloride ions. At pH values below the PZC, the surface of the adsorbent will be positively charged, which could enhance the electrostatic attraction with the negatively charged chloride ions, facilitating adsorption. Conversely, at pH values above the PZC, the surface will be negatively charged, potentially leading to electrostatic repulsion with the chloride ions[52,53]. In this study, the pH_{pzc} for AgMX has been obtained 3.25 as it is illustrated in Fig. S1., but considering the pH of various solution of NaCl with different concentration, the pH of solution

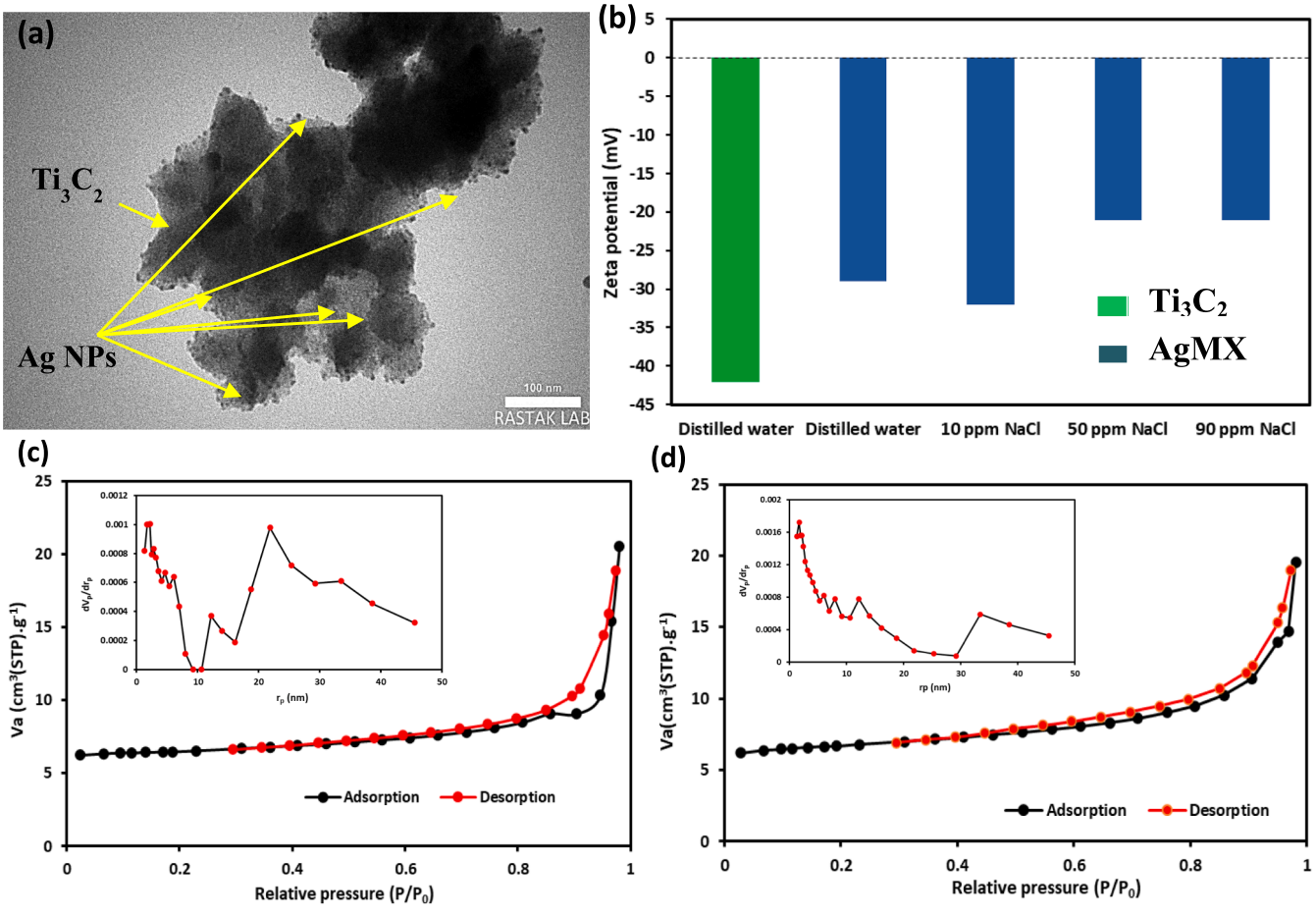

Fig. 4. TEM image of a) AgMX, b) Zeta potential measurement of Ti_3C_3 and AgMX, and N_2 ad(de)sorption isotherms for c) Ti_3C_2 and d) AgMX.

is above the pH_{pzc}, hence the surface charge of adsorbent still remains negative[54–57].

3.3. BET analysis

Table S2 showcases the outcomes obtained through BET analysis applied to each of the synthesised Ti_3C_2 and AgMX samples. As indicated in Table S2, the Ti_3C_2 sample's specific surface area, diameter, and pore volume were determined to be 23.9 m2/mg, 5.29 nm, and 0.03 cm3/g, respectively. These findings provide robust confirmation of the elevated surface area owing to the two-dimensional architecture of Ti_3C_2, revealing discernible pores distributed across its plane surfaces. Furthermore, TEM investigations revealed the uniform coverage of silver nanoparticles across the Ti_3C_2 surface after its modification with silver nitrate. These nanoparticles exhibited a spherical morphology, albeit with a smaller specific surface area compared to the sheet-like structure of Ti_3C_2. Complementarily, SEM observations highlighted the multi-layered nature of the MXene used in the study. Notably, the size of the silver nanoparticles exceeded the interlayer distance between the Ti_3C_2 sheets, which typically spans a few angstroms. Consequently, the silver nanoparticles effectively enveloped the Ti_3C_2 surface, without permeating between the layers, forming a wall-like structure on the Ti_3C_2 surface. This resulted in a reduced specific surface area of 17.37 m^2/mg for the silver nitrate-modified Ti_3C_2, a contrast to the planar Ti_3C_2 structure. Further insights were collected from the determination of the AgMX's pore volume and diameter, corresponding to 0.0302 cm3/g and 6.966 nm, respectively. These outcomes imply that the silver nanoparticles partially occupied the surface pores of Ti_3C_2, inducing a decline in pore volume. The observed enlargement in pore size from 5.2907 nm to 6.966 nm can be linked to the inverse relationship between pore size and BET surface area. Fig. 4c, d demonstrates the N_2 ad(de)sorption isotherm and the particle size distribution curve of the Ti_3C_2 and AgMX. The results show that the N_2 ad(de)sorption isotherm for both samples is belonged to type IV, which indicate their mesoporous and a layered structure within the synthesized nano-adsorbent [58].

3.4. DOE-based chloride removal testing

The investigational design for eliminating chloride ion and the corresponding results attained using the Design-Expert software are summarised in Table S3. The effect of each parameter and their interactions on the process is assessed through Analysis of Variance (ANOVA). The two key metrics used to evaluate the influence of individual parameter on the last model are the P-value and F-value. Higher F-values and lower P-values (below 0.05) indicate a greater significance of the variable in determining the final outcome. The Lack of Fit value, which is greater than 0.05, along with a P-value less than 0.05, confirms the suitability of the selected model for accurately predicting the final results. Moreover, the adsorbent dose and time exhibit the highest F-values among the parameters (as shown in Table S4), suggesting their pivotal role in the prediction process. It is important to note that the test data are assumed to follow a normal distribution. To verify this assumption, the ratio of the highest to the lowest percentage of chloride ion removal should be less than 10. In this project, the ratio is calculated as 2.19, with the highest and lowest values of 91.81 % and 41.9 %, respectively.

During the experimental process, diagnostic plots were utilised to assess the accuracy and validity of the model as depicted in Fig. 5. The normal probability distribution of the externally studentised residuals was displayed in Fig. 5a, with most of the points aligning along a straight line. This indicates that no transformations are required for the predicted responses. As it is illustrated in Fig. 5b which demonstrates the favourable agreement between the actual responses and the predicted values, indicating the high accuracy of the model proposed by the software using CCD. In Fig. S2b, the residuals plot based on the test number is presented. The dispersion of the data should ideally exhibit a random pattern without any discernible upward or downward trend. The observed pattern in Fig. S2b aligns with this expectation, further affirming the suitability of the CCD model for accurately modelling chloride ion removal. Moreover, the Box-Cox diagram in Fig. 5c confirms the normality of the data. Since (λ) is equal to 1, the extra power conversion is not essential for the model. Based on the analysis performed using the Design-Expert software, the quadratic model, represented by the second-order polynomial equation (Eq. (2)-taken from Anova Table, Table S4), is suggested as the most suitable method for predicting the removal of chloride ions using AgMX. In this equation, the parameters A, B, and C correspond to the adsorbent dosage, time, and initial chloride ion concentration, respectively. It is noted that terms with a high value, positive sign (+) or both preceding the direct and quadratic terms signifies their positive and increasing influence and conversely, high value, negative sign (-) or both exert an opposite effect on the process efficiency.

$$\text{Removal}\,(\%) = (82.05) + (12.26 \times A) + (1.76 \times B) - (1.54 \times C) + (1.11 \times A \times B) + (3.30 \times A \times C) - (0.4313 \times B \times C) - \left(3.79 \times A^2\right) - \left(1.76 \times B^2\right) - \left(6.56 \times C^2\right) \quad (2)$$

To solve Eq. (2). the Solver Add-Ins in Microsoft Excel software was implemented to forecast the essential values for highest adsorption of chloride ions (optimization results), and the optimization result is shown in Fig. S3. The optimized predicted value (91.76 %) was assessed in both experimental and operational conditions to evaluate the adequacy of the model in predicting the response, and the determined average result of 3 replicates as the actual chloride removal (91.8 %) was examined.

The influence of every individual parameter is depicted in Fig. 5, where the adsorbent dose, time, and primary concentration of chloride demonstrate F-values of 2151.25, 49.74, and 37.73, respectively, indicating their substantial impact on the response of the process. Fig. 5d illustrates the effect of adsorbent dosage on chloride ion removal percentage. It is evident that increasing the different dose of adsorbent from 0.2 to 2 g/L results in a corresponding increase on eliminating chloride ion. This can be attributed to the availability of more active sites for pollutant absorption, thereby enhancing the removal efficiency. Notably, a substantial 50 % chloride ion removal can be achieved by adding less than 2 g/L of adsorbent within 9 min. In Fig. 5e, the impact of time on chloride ion elimination is depicted. It is observed that, with an adsorbent dosage of 1.1 g/L and a pollutant concentration of 50 mg/L, variations in the time range of 1 to 17 min have a minimal effect on the amount of chloride removal. This can be attributed to the high activity of vacant adsorbent sites that quickly interact with chloride ions, leading to surface adsorption and occupation of these active sites. Thus, a slight upward slope is observed in the chart during the 1 to 10-minute range, followed by a semi-steady state. Fig. 5f presents the influence of initial chloride concentration on the removal percentage. The results indicate that at lower initial chloride concentrations, adsorption of chloride ions primarily occurs at vacant adsorbent surface sites, resulting in a 20 % removal rate. However, as the concentration of chloride ion rises from 50 to 90 mg/L, the adsorption capacity diminishes. This decrease in adsorption can be attributed to the saturation of active absorption sites following an increase in the initial chloride concentration.

3.5. Combined effects: Adsorbent dose and chloride concentration

The DOE software lets the investigation of selected parameters interactions and the effects these interactions have on the final response which here is considered the adsorption capacity. Two types of plots are frequently used in these investigations which are contour and three-dimensional plots. The contour ones are applied to illustrate the level of interaction between the selected factors, with a circular shape indicating minimal interaction and elliptical or saddle shapes indicating

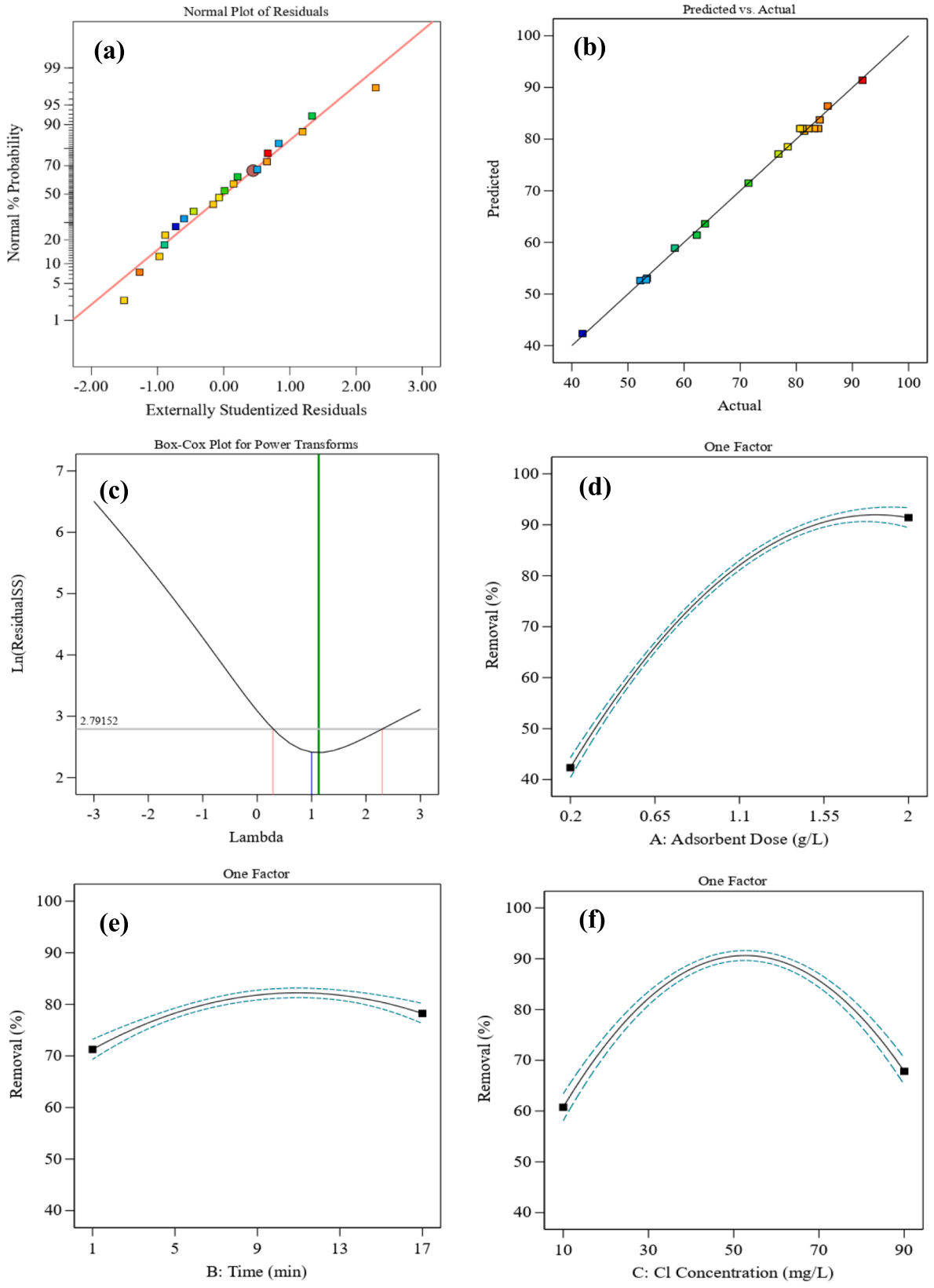

Fig. 5. (a) Normal scheme of residuals, (b) actual vs. predicted plot, (c) Box-Cox scheme for power convert, (d) Removal vs. adsorbent dose, (e) removal vs. time and (f) removal vs. primary chloride ion concentration one factor plots.

significant interaction. Three-dimensional plots are also used to gain a deeper understanding of these interactions, with colors ranging from red representing high effect of interaction to blue indicating less degree of interaction and effect on the efficiency of chloride removal. Contour and 3D plots in Fig. 6 illustrate the simultaneous effect of key parameters including primary chloride ion concentration, adsorbent dose and contact time on chloride removal efficiency.

Fig. 6a, d and g illustrate the combined effect of adsorbent dosage (ranging 0.2–2.0 g/L) and the initial concentration of chloride ions (ranging 10–90 ppm) on the yield of chloride removal. Based on the ANOVA findings and the F-value reported in Table S4 (F-value = 87.05), it can be concluded that the interaction between these two variables is statistically significant. Fig. 6a demonstrates that the effectiveness of chloride ion removal is increased at both up and below chloride ion concentrations due to the enhanced surface area and the presence of more energetic adsorption places resulting from an increase in the adsorbent dosage. At an initial chloride concentration of 70 mg/L, the upward trend is steeper, and the removal percentage increases from 30 % to 85 %. In contrast, at 30 mg/L, only a 30 % removal is observed. Overall, increasing the adsorbent dosage leads to higher removal percentages. The contour and 3D plots (Fig. 6d and g) indicate that the red points represent removal rates above 90 %, while the blue points correspond to removal rates below 60 %. A removal percentage beyond 90 % is attained with a high adsorbent dose (>1.55 g/L) and a chloride ion concentration of 50 mg/L. Generally, higher adsorbent dosages (>1.55 g/L) are required at higher chloride ion concentrations (70–90 mg/L) to reach a high percentage of eliminating chloride ion.

3.6. Combined effects: Adsorbent dose and time

Fig. 6b, e and h illustrate the combined influence of adsorbent dosage (ranging 0.2–2.0 g/L) and time (ranging 1–17 min) at a constant initial concentration of chloride ions (50 mg/L) on the removal of chloride ions. As shown in Fig. 6a, increasing the adsorbent dosage leads to an enhanced removal trend, both at a short time of 5 min and a longer at 13 min. At a low dosage of 0.65 g/L, both graphs exhibit the same removal percentage of 65 %. However, with a higher dosage of the adsorbent, the impact of time becomes more apparent. For instance, at an adsorbent dosage of 1.55 g/L, the difference in removal percentage due to varying reaction times reaches 10 %. The 3D and contour graphs (Fig. 6e and h)

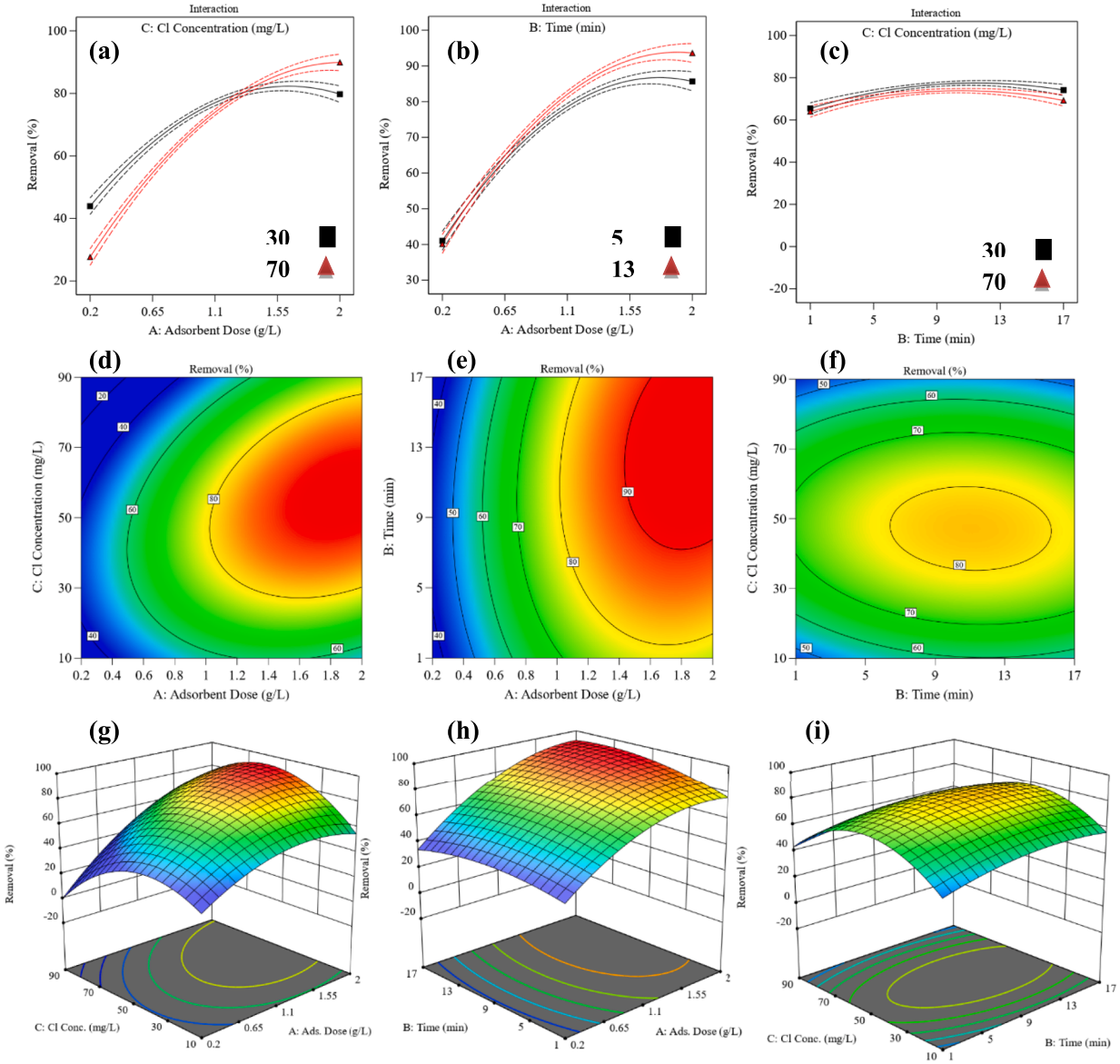

Fig. 6. (a-i) graph, counter, and 3D plots of the simultaneous interaction of parameters on the chloride ion removal, respectively.

demonstrate that a removal percentage higher than 90 % can be achieved by simultaneously increasing both parameters. At low adsorbent dosages for all time intervals (1 to 17 min), the percentage of removal remains below 50 % and is primarily located in the blue zone. For example, with an adsorbent dosage of 0.65 g/L and a contact time of 13 min, only 64 % of chloride ions is removed.

3.7. Combined effects: Chloride concentration and time

Fig. 6c, f and i depict the combined effect of chloride concentration and contact time on the percentage of chloride ion removal at a constant adsorbate dosage of 1.1 g/L. As observed in Fig. 6c, both graphs for chloride concentrations of 30 and 70 mg/L display a gradual slope and are closely aligned, suggesting that contact time has minimal impact on chloride removal. It can be inferred that the removal of chloride ions is not significantly influenced by the duration of contact. For instance, when the initial chloride concentration is 30 mg/L and the adsorbent dosage is 1.1 g/L, only a slight 3–5 % removal of chloride ions is achieved. Additionally, the contour and 3-dimensional plots (Fig. 6f and i) do not exhibit a region with a high removal percentage of 90 % or above. Instead, other coloured areas are observed, corresponding to removal percentages of approximately 50 % to 72 %. Hence, it can be concluded that the interaction between these two parameters has the least effect on the percentage of removal, which aligns with the results presented in Table S4 (F-value BC = 1.33).

3.8. Removal optimisation

Cost-effectiveness is a pivotal factor for commercialisation of materials synthesis demanding optimisation of both time and costs throughout the entire process. To pinpoint the most efficient conditions for chloride ion removal, the Design Expert software was used to optimise various parameters which have been found of significance including adsorbent dose, primary chloride ion concentration, reaction time, and chloride ion elimination. For this purpose, determining the goal values of three main parameter in range and the chloride ion removal at maximum desired value, the adsorbent dosage was manipulated within 0.65–1.55 g/L, while the chloride ion concentration was between 30 and 70 mg/L. The contact time spanned between 5 and 13 min and maximum chloride ion removal, deemed the most crucial parameter. Fig. S3 visually represents the optimisation process towards the identification of the optimal point at an adsorbent dosage of 1.55 g/L, a contact time of 12.19 min, and a primary chloride ion concentration of 52.17 mg/L. Implementation of these optimised parameters led to a chloride ion removal of 91.76 %, aligning with the highest experimentally obtained response of 91.8 % and a desirability value of 0.999. With a desirability value of 0.98, the predicted function effectively mirrors the favourable conditions and experimental model. The optimization test was carried two more times in order to check the repetitiveness of the responses and the results obtained were 92.13 % and 91.28 %, respectively.

3.9. Adsorption mechanisms

Langmuir [59,60], Freundlich [61] and Dubinin-Kaganer-Radushkevich (DKR) [53] models were used to study the underlying adsorption mechanisms of the chloride removal. The Langmuir and Freundlich models are two-parameter isotherms that offer a reliable and comprehensive description of the experimental performance over a wide range of conditions. The DKR model used to explain energetic heterogeneity of solid surface at the monolayer region in micropores. The type of physical adsorption has an E value in the range of 1–8 kJ/mol and the chemical adsorption E value is more than 8 kJ/mol.

Regarding to the results obtained for coefficient for both models (R^2) in Table S5, it can be seen that Langmuir's is substantially greater than Freundlich's and DKR's, and is closer to 1, resulting in Langmuir's better expressing capability for the interaction between adsorbent and pollutant. The Langmuir model portrays more desired and acceptable R^2 value (0.98) than both the Freundlich and DKR models (0.94) (Fig. S4 a, b and c). Fig. S5 presents the calculated values of R_L, in the range between 0.90 and 0.50, proving the satisfactory of the adsorption process. The value of R_L reflects the degree of irreversibility in the system and provides a qualitative assessment of the interactions that occurs between adsorbent and the adsorbate. As the value approaches zero, it signifies an ideal irreversible state, while a value of 1 represents a reversible state. The AgMX adsorbent demonstrated a maximum monolayer adsorption capacity (q_m) of 250 mg/g. Table 1 compares the highest capability of adsorption for the AgMX adsorbent with those reported in other studies. According to the values reported for q_m, the AgMX exhibits exceptional efficiency and competitive performance for chloride ions removal from aqueous media. As it is shown in Table S5, β is 0.48 kJ/mol for AgMX which means that chloride adsorption on AgMX follow the physisorption process in our study because the sorption energy found below 8 kJ/mol.

As depicted in Fig. S4d, the adsorption capacity vs. time plot under the circumstances with the concentration of 51.4 mg/L for chloride ion, adsorbent dose of 1.55 g/L, and 15 min of contact was evaluated. In the early times, the slope of the graph is steeper, which indicates the higher rate of absorption due to the abundance of active absorption sites. With the passage of time, as it is clear in the Fig. S4d, the rate of adsorption decayed and touched the equilibrium stage gradually, which saturation of active sites can be the reason for this phenomenon.

The study of the kinetics of adsorption kinetics was implemented applying adsorption kinetic models as illustrated in Fig. S4 e-h. In this regard four recognized kinetic models: the pseudo-first-order, the pseudo-second-order, Elovich and Intraparticle diffusion were used to investigate the kinetics of chloride ion adsorption by the AgMX in and the results are shown in Fig. S4e and f. The obtained regression coefficients and constant rates for all four models are presented in Table S6. According to previous studies, it is observed that the experimental data exhibit a higher correlation coefficient value of 0.98 in the pseudo-second-order kinetic model, compared to the pseudo-first-order, Elovich and Intraparticle diffusion models ($R^2 = 0.2335, 0.1212$ and 0.2050 respectively). This finding confirms that the adsorption of chloride ions from water by AgMX follows the pseudo-second-order model. Furthermore, the calculated value of q (qe, cal = 26.595) using the pseudo-second-order model closely matches the experimental q value (qe, exp = 30.18), indicating consistency between these two values. Therefore, the pseudo-second-order model provides a more accurate description of the adsorption of chloride ions using AgMX compared to the other model. The surface adsorption, including chemisorption, is the limiting factor in this model, where the removal of a substance from a solution is attributed to the physiochemical interactions between the two phases[62].

During the removal of chloride ions by silver-modified Ti_3C_2 MXene adsorbent from water, a series of chemical reactions may take place. As it is illustrated in Fig. 7, the silver species on the Ti_3C_2 MXene surface can interact with chloride ions through electrostatic interactions, leading to the formation of silver chloride complexes on the adsorbent surface which could be separated through precipitation due the high k_{sp} of the formed AgCl complexes[35,68]. Ion exchange mechanisms may also

Table 1
Comparing the removal capacity of the AgMX with other adsorbents reported in the literature for chloride ion adsorption.

Adsorbent	Uptake capacity ($mg.g^{-1}$)	Reference
bentonite modified by Ag NPs	107.64	[63]
ZnAl-NO_3 layered double hydroxides	169.3	[64]
CLDH ($Mg_{0.80}Al_{0.20}O_{1.1}$)	149.5	[65]
MgAl-LDHs	24.85	[66]
Mg–Al oxide	29.76	[67]
Ag NPs-modified MXene	250	**Current study**

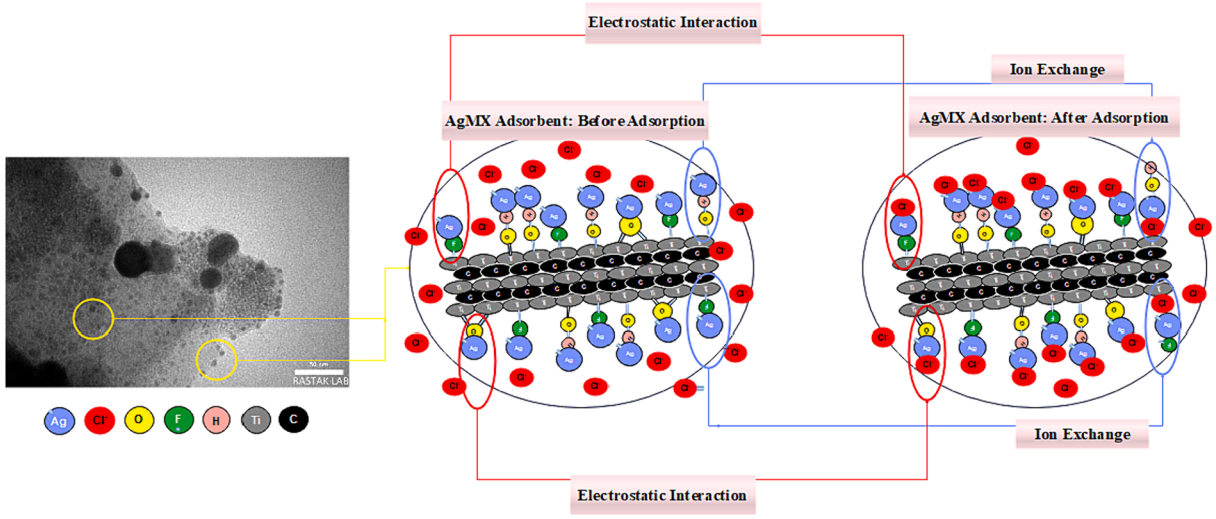

Fig. 7. The interactions that occur during the process of removing chloride ions from water using AgMX adsorbent. Electrostatic interaction which occurs as a result of interaction between positively charged silver nanoparticles with Cl^- and also ion exchange by substitution of Cl^- with the elements of termination groups followed by electrostatic attraction with positively charged silver nanoparticles.

occur, where the silver chloride complex exchanges with ions in the solution, facilitating the removal of chloride ions[69–71]. When the adsorbent is equipped with fluorine and hydroxyl termination groups, the ion exchange process on the surface becomes more intricate. The fluorine termination groups may interact with chloride ions through electrostatic forces, promoting adsorption, while the hydroxyl termination groups provide active sites for ion exchange, and the Cl^- species in the media exchange their position with the mentioned species and provide new termination groups on the surface on the adsorbent, interacting with the silver nano particles and enhancing the overall removal efficiency of chloride ions from water. In the following equations, the general reactions of formation of AgMX using dry-impregnation method are proposed[72–75].

$$AgNO_3 + H_2O \rightarrow Ag^+ + NO_3^- + H_2O \tag{3}$$

$$Ag_n^+ + Ti_3C_2(O)^- + Ti_3C_2(F)^- + Ti_3C_2(OH)^- \rightarrow Ti_3C_2O(Ag) + Ti_3C_2F(Ag) + Ti_3C_2OH(Ag) \tag{4}$$

$$NaCl + H_2O \rightarrow Na^+ + Cl^- + H_2O \tag{5}$$

$$Ti_3C_2O(Ag) + Ti_3C_2F(Ag) + Ti_3C_2OH(Ag) + Cl_n^- \rightarrow Ti_3C_2O(AgCl) + Ti_3C_2F(AgCl) + Ti_3C_2OH(AgCl) \tag{6}$$

Furthermore, during the removal of chloride ions by AgMX adsorbent from water, the chloride selectivity can be a crucial aspect. The specific interaction between chloride ions and the silver species on the adsorbent surface can provide high selectivity for chloride ion removal in aqueous media[76]. When chloride ions come into contact with the silver species on the adsorbent surface, a unique and strong interaction occurs, facilitating the preferential adsorption of chloride ions[77,78]. Additionally, the presence of terminal groups such as fluorine and hydroxyl on the adsorbent surface may contribute to chloride selectivity, allowing for specific interactions that favor the selective adsorption of chloride ions by ion exchange over other ions present in the water[53]. This chloride selectivity by the adsorbent can be essential for water purification applications and treatment of effluents contaminated with chloride ions [79]. These terminal groups can form specific interactions with chloride ions, creating favorable conditions for the selective removal of chloride ions while minimizing the adsorption of other ions present in the water. This targeted interaction mechanism contributes to the effectiveness and efficiency of chloride ion removal by the adsorbent in aqueous environments[80–82].

3.10. Comparison of chloride ion removal performance by Ti_3C_2 MXene adsorbent before and after modification by $AgNO_3$

In order to investigate and compare the performance of Ti_3C_2 MXene in chloride ion removal before and after modification with silver nanoparticles, two experiments were performed in the optimal conditions suggested by the DOE software, followed by an experiment using the AgMX in chloride ion removal from real sample taken from tap water and determining the adsorption performance. As it is exhibited in the Fig. S6, the adsorbent modified by silver nanoparticles has a much higher ability than the unmodified adsorbent in removing chloride ions, and this is due to the presence of silver nanoparticles on the surface, proposing active sites for absorption, supported by electrostatic attraction, as it was discussed before. The removal percentage by the adsorbent has increased to 91.81 % compared to the unmodified state which showed a weak ability in chloride ion removal equal to 20 %. Moreover, in the real sample experiment in which adsorbent dose and time, were similar to the optimum condition, 81.37 % chloride ion removal was obtained, showing a promising adsorption capability that makes the adsorbent suitable to be used in various practical applications.

3.11. Reusability and regeneration

To evaluate the performance of the adsorbent for practical applications in industrial settings, two procedures were chosen to test the reusability and also the regeneration capability of the adsorbent. The experiments were conducted over four cycles to ensure consistency of the results. Two diverse methods were employed to explore the functionality and reusability of the adsorbent in order to chloride ion exclusion: (1) reusing the adsorbent without any further preparation and (2) regeneration of the adsorbent through rinsing by a solvent. For the reusability approach, the AgMX adsorbent was utilized without any additional treatment or modification after each cycle. Fig. 8 illustrates the chloride ion removal efficiency of the adsorbent over four cycles. It can be recorded that the effectiveness of adsorption declined to 82.48 %, 73.15 %, and 68.15 % in the second, third, and fourth cycles, respectively. This decrease in removal efficiency can be attributed to the deactivation of the AgMX surface, which occurs during the chloride ion adsorption process. In the second approach, the regeneration of the AgMX adsorbent was examined using an economical solvent, NaOH

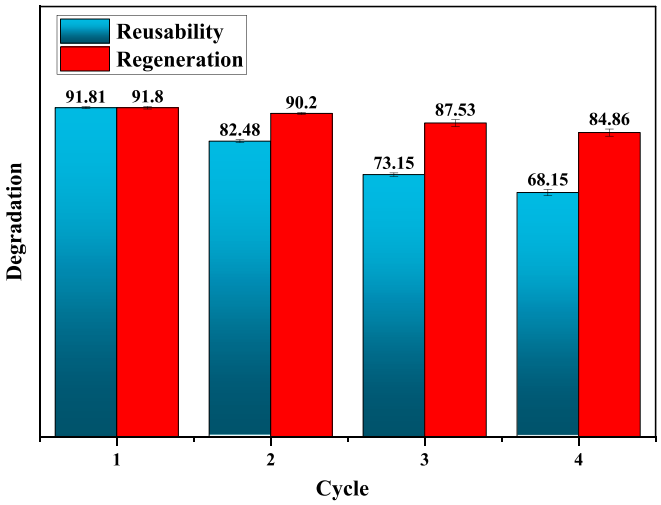

Fig. 8. The result of adsorption for reusability and regeneration experiments setting the following conditions: initial concentration of chloride ion equal to 51.49 mg/L and 1.55 g/L adsorbent dose at 9.6 min of contact time.

solution, and distilled water. After operating each individual adsorption cycle, the adsorbent was rinsed with a 0.4 M sodium hydroxide solution for 30 min, followed by rinsing with distilled water and drying at 90 °C for 20 min. The regenerated adsorbent was then brought into contact with fresh water containing chloride ions for the subsequent cycle. Fig. 8 demonstrates the removal efficiency of the adsorbent using this regeneration method. As it is depicted, the efficiency of removal declined slowly from cycle to cycle and after four cycles, the removal efficiency of the AgMX, which underwent treatment with NaOH solution, decreased from 91.81 % to 84.86 %. Thus, washing the adsorbent with a solvent over multiple cycles proved to be more effective, resulting in a higher removal percentage compared to the untreated or unmodified adsorbent.

4. Conclusion

The current study aimed to evaluate the efficiency of newly synthesised AgMX composite for the chloride ion removal from water. The nanocomposite was synthesised through dry impregnation methods, and characterised using various techniques, including XRD, SEM, EDS, TEM, BET, Zeta potential and ionic chromatography analysis, which confirmed the successful synthesis of the nanocomposite. Experiments were optimised based on a variety of adsorption operating conditions including adsorbent dose, reaction time and chloride ion concentration using the RSM-CCD techniques. The adsorbent dosage was found to have the highest impact, while chloride concentration has the least F-value. The optimum conditions were found at adsorbent dosage: 1.55 g/L, reaction time: 12.19 min and chloride concentration: 52.17 mg/L, leading to 91.8 % removal, while 81.37 % chloride ion adsorption was obtained in real sample experiment. The Langmuir adsorption mechanism was the best fit affirming a phonically adsorption and layer by layer with the highest adsorption capacity of 250 mg/g and showed the best fit to adsorption isotherm (R^2:9852) comparing to Freundlich and Dubinin-Kaganer-Radushkevich (DKR) isotherms. The pseudo-second-order kinetic model offered the closest data to the experimental results (R^2:9893) compared to the pseudo-first-order, Elovich and Intraparticle diffusion models ($R^2 = 0.2335,\ 0.1212$ and 0.2050), respectively. The stability of AgMX during the adsorption process was examined over four cycles, revealing minimal leaching of Ag. The synthesised AgMX showed notable advantages in terms of high efficiency in chloride ion removal and potential for regeneration as a suitable adsorbent for the removal of chloride ions. When compared to the documented research, AgMX demonstrated a significantly higher maximum adsorption uptake for chloride ions with the need for further investigation into the chloride ion selectivity and stability in more outdoor aqueous medias along with a comparative analysis of its economic efficiency to other commercial adsorbents. Moreover, the potential hazardous effects of AgMX, including toxicity and other environmental risks, should be studied.

CRediT authorship contribution statement

Roya Moosaei: Writing – original draft, Visualization, Methodology, Investigation, Formal analysis, Conceptualization. **Samad Sabbaghi:** Writing – review & editing, Validation, Supervision, Resources, Project administration, Methodology, Investigation, Formal analysis, Conceptualization. **Mohammad Sadegh Jafari Zadegan:** Methodology, Investigation, Formal analysis. **Kamal Rasouli:** Methodology, Investigation, Formal analysis. **Samaneh Ghaedi:** Writing – review & editing, Visualization, Validation, Methodology, Investigation, Formal analysis, Conceptualization. **Hamid Rajabi:** Writing – review & editing, Visualization, Validation, Supervision, Resources, Project administration, Methodology, Investigation, Funding acquisition, Formal analysis, Conceptualization.

Declaration of competing interest

The authors declare that they have no known competing financial interests or personal relationships that could have appeared to influence the work reported in this paper.

Data availability

Data will be made available on request.

Appendix A. Supplementary data

Supplementary data to this article can be found online at https://doi.org/10.1016/j.molliq.2024.124480.

References

[1] M. Mohammadi, S. Sabbaghi, M. Binazadeh, S. Ghaedi, H. Rajabi, Chemosphere (2023) 139311.
[2] A. Moridi, S. Sabbaghi, J. Rasouli, K. Rasouli, S.A. Hashemi, W.-H. Chiang, S. M. Mousavi, Water 15 (2023) 1819.
[3] Z. Suiyi, R. Yanong, Z. Yuxin, Z. Minglin, Y. Weilu, X. Xinfeng, Y. Yang, L. Jiancong, Q. Zhan, L. Jialin, C. Yu, J. Environ. Chem. Eng. 12 (2024) 112024.
[4] M. Esfandiaribayat, M. Binazadeh, S. Sabbaghi, M. Mohammadi, S. Ghaedi, H. Rajabi, Sci. Rep. 14 (2024) 1163.
[5] A. Naderipour, S.A. Nowdeh, M. Babanezhad, E.S. Najmi, H. Kamyab, Z. Abdul-Malek, Environ. Sci. Pollut. Res. (2021) 1.
[6] Y.A.B. Neolaka, Y. Lawa, J. Naat, A.C. Lalang, B.A. Widyaningrum, G.F. Ngasu, K. A. Niga, H. Darmokoesoemo, M. Iqbal, H.S. Kusuma, Results in Engineering 17 (2023) 100824.
[7] S. Ghaedi, K. Seifpanahi-Shabani, M. Sillanpää, Chemosphere 292 (2022) 133412.
[8] M. Binazadeh, J. Rasouli, S. Sabbaghi, S.M. Mousavi, S.A. Hashemi, C.W. Lai, Materials 16 (2023) 3526.
[9] Y. Xue, Y. Ma, G. Long, H. He, Z. Li, Z. Yan, J. Wan, S. Zhang, B. Zhu, J. Sea Res. 193 (2023) 102380.
[10] K. Rasouli, J. Rasouli, M.S. Mohtaram, S. Sabbaghi, H. Kamyab, H. Moradi, S. Chelliapan, J. Clean. Prod. 419 (2023) 138181.
[11] N. Yousefi Limaee, M. Ghahari, K. Seifpanahi-Shabani, A. Naeimi, S. Ghaedi, Prog. Color Color. Coat. 16 (2023) 1.
[12] V.V. Wanatasanappan, P.K. Kanti, P. Sharma, N. Husna, M. Abdullah, J. Mol. Liq. 375 (2023) 121365.
[13] P.K. Kanti, P. Sharma, K. Sharma, M. Maiya, J. Energy Chem. 82 (2023) 359.
[14] Y. Xue, X. Liu, N. Zhang, Y. Shao, C.C. Xu, International journal of minerals, Metallurgy and Materials 30 (2023) 2364.
[15] A.A. Sattar, Water Conservation and Management 5 (2021) 1.
[16] T. Kameda, T. Yoshioka, T. Mitsuhashi, M. Uchida, A. Okuwaki, Water Res. 37 (2003) 4045.
[17] Y. Xue, T. Yang, X. Liu, Z. Cao, J. Gu, Y. Wang, Chemosphere 342 (2023) 140164.
[18] S.S. Kaushal, ACS Publications, 2016.
[19] G.L. Dotto, G. McKay, J. Environ. Chem. Eng. 8 (2020) 103988.
[20] R.J. Bauer, CPT: pharmacometrics & systems pharmacology 8 (2019) 538.
[21] M. Tayefeh, J. Storage Mater. 52 (2022) 105025.
[22] M. Prajapati, M. Shah, B. Soni, Groundw. Sustain. Dev. (2022) 100808.

[23] E.P. Kuncoro, T. Soedarti, T.W.C. Putranto, H. Darmokoesoemo, N.R. Abadi, H. S. Kusuma, Data Brief 16 (2018) 908.
[24] R.A. Khera, M. Iqbal, A. Ahmad, S.M. Hassan, A. Nazir, A. Kausar, H.S. Kusuma, J. Niasr, N. Masood, U. Younas, Desalin. Water Treat. 201 (2020) 289.
[25] J.N. Naat, Y.A. Neolaka, T. Lapailaka, R.T. Tj, A. Sabarudin, H. Darmokoesoemo, H.S. Kusuma, Rasayan J. Chem. 14 (2021) 550.
[26] H.S. Kusuma, N. Illiyanasafa, D.E.C. Jaya, H. Darmokoesoemo, N.R. Putra, Sustain. Chem. Pharm. 37 (2024) 101346.
[27] Y.A. Neolaka, A.A. Riwu, U.O. Aigbe, K.E. Ukhurebor, R.B. Onyancha, H. Darmokoesoemo, H.S. Kusuma, Results in Chemistry 5 (2023) 100711.
[28] C. Wang, P. Shi, C. Guo, R. Guo, J. Qiu, J. Electroanal. Chem. 956 (2024) 118072.
[29] W. Liu, F. Huang, Y. Liao, J. Zhang, G. Ren, Z. Zhuang, J. Zhen, Z. Lin, C. Wang, Angew. Chem. 120 (2008) 5701.
[30] D. Abdissa, K. Beyecha, (2021).
[31] T. Qiang, B. Qiu, L. Chen, L. Ren, Available at SSRN 4137010.
[32] P.D. Indurkar, S.K. Raj, V. Kulshrestha, Environ. Sci. Pollut. Res. (2023) 1.
[33] X. Zhao, B. Fan, N. Qiao, R.A. Soomro, R. Zhang, B. Xu, Appl. Surf. Sci. 642 (2024) 158639.
[34] Y. Zhang, J. Luo, B. Feng, H. Xu, Y. Sun, X. Gu, X. Hu, M. Naushad, B. Gao, H. Ren, Environ. Pollut. 330 (2023) 121777.
[35] R.P. Pandey, K. Rasool, V.E. Madhavan, B. Aïssa, Y. Gogotsi, K.A. Mahmoud, J. Mater. Chem. A 6 (2018) 3522.
[36] M.A. Islam, M.V. Jacob, E. Antunes, J. Environ. Manage. 281 (2021) 111918.
[37] Y. Zhen, V.S. Reddy, B. Ramasubramanian, S. Ramakrishna, J. Mater. Sci. 57 (2022) 21960.
[38] M. Galedari, M.M. Ghazi, S.R. Mirmasoomi, Chem. Eng. Res. Des. 145 (2019) 323.
[39] H.S. Kusuma, A.N. Amenaghawon, H. Darmokoesoemo, Y.A. Neolaka, B. A. Widyaningrum, C.L. Anyalewechi, P.I. Orukpe, Environ. Technol. Innov. 24 (2021) 102005.
[40] M.M. Bakry, S.S. Salem, H.M. Atta, M.S. El-Gamal, A. Fouda, Egypt. J. Chem. 66 (2023) 371.
[41] A. Dank, T. Abee, E.J. Smid, Curr. Opin. Food Sci. (2023) 101048.
[42] K. Rasool, R.P. Pandey, P.A. Rasheed, S. Buczek, Y. Gogotsi, K.A. Mahmoud, Mater. Today 30 (2019) 80.
[43] X. Sheng, S. Li, H. Huang, Y. Zhao, Y. Chen, L. Zhang, D. Xie, J. Mater. Sci. 56 (2021) 4212.
[44] M. Alhabeb, K. Maleski, B. Anasori, P. Lelyukh, L. Clark, S. Sin, Y. Gogotsi, Chem. Mater. 29 (2017) 7633.
[45] Z. Li, L. Wang, D. Sun, Y. Zhang, B. Liu, Q. Hu, A. Zhou, Mater. Sci. Eng. B 191 (2015) 33.
[46] L. Li, N. Zhang, M. Zhang, L. Wu, X. Zhang, Z. Zhang, ACS Sustain. Chem. Eng. 6 (2018) 7442.
[47] Z. Zhang, Z. Cai, Y. Zhang, Y. Peng, Z. Wang, L. Xia, S. Ma, Z. Yin, R. Wang, Y. Cao, Carbon 174 (2021) 484.
[48] K. Rasouli, A. Alamdari, S. Sabbaghi, Sep. Purif. Technol. 307 (2023) 122799.
[49] B. Anasori, M.R. Lukatskaya, Y. Gogotsi, Nat. Rev. Mater. 2 (2017) 1.
[50] J. Wang, D. Zhi, H. Zhou, X. He, D. Zhang, Water Res. 137 (2018) 324.
[51] R. Hunter, New York, USA (1981).
[52] E.P. Kuncoro, D.R.M. Isnadina, H. Darmokoesoemo, O.R. Fauziah, H.S. Kusuma, Data in brief 16 (2018) 622.
[53] Y.A. Neolaka, Y. Lawa, J. Naat, A.A. Riwu, Y.E. Lindu, H. Darmokoesoemo, B. A. Widyaningrum, M. Iqbal, H.S. Kusuma, React. Funct. Polym. 166 (2021) 105000.
[54] A. Rozmysłowska-Wojciechowska, J. Mitrzak, A. Szuplewska, M. Chudy, J. Woźniak, M. Petrus, T. Wojciechowski, A.S. Vasilchenko, A.M. Jastrzębska, Materials 13 (2020) 2347.
[55] E. Lasareva, A. Parfenova, M. Beklemishev, Biointerface Research in Applied Chemistry 10 (2019) 4922.
[56] Y. Ying, Y. Liu, X. Wang, Y. Mao, W. Cao, P. Hu, X. Peng, ACS Appl. Mater. Interfaces 7 (2015) 1795.
[57] Y. Du, B. Yu, L. Wei, Y. Wang, X. Zhang, S. Ye, J. Mater. Sci. 54 (2019) 13283.
[58] P. Karthikeyan, S.S. Elanchezhiyan, J. Preethi, K. Talukdar, S. Meenakshi, C. M. Park, Ceram. Int. 47 (2021) 732.
[59] A. Ayub, Z.A. Raza, M.I. Majeed, M.R. Tariq, A. Irfan, Int. J. Biol. Macromol. 163 (2020) 603.
[60] N. Ayawei, A.N. Ebelegi, D. Wankasi, J. Chem. 2017 (2017).
[61] J. Wang, X. Guo, Chemosphere 258 (2020) 127279.
[62] Y.A. Neolaka, Y. Lawa, J. Naat, A.A. Riwu, A.W. Mango, H. Darmokoesoemo, B. A. Widyaningrum, M. Iqbal, H.S. Kusuma, J. Mater. Res. Technol. 18 (2022) 2896.
[63] H. Moradi, S. Sabbaghi, N.S. Mirbagheri, P. Chen, K. Rasouli, H. Kamyab, S. Chelliapan, Environ. Res. (2023) 115484.
[64] L. Lv, P. Sun, Z. Gu, H. Du, X. Pang, X. Tao, R. Xu, L. Xu, J. Hazard. Mater. 161 (2009) 1444.
[65] L. Lü, J. He, M. Wei, Water Res. 40 (2006) 735.
[66] J. Wei, J. Xu, Y. Mei, Q. Tan, Appl. Clay Sci. 187 (2020) 105495.
[67] R. Hamidi, P. Kazemi, Desalin. Water Treat. 54 (2015) 332.
[68] G. Zou, Z. Zhang, J. Guo, B. Liu, Q. Zhang, C. Fernandez, Q. Peng, ACS Appl. Mater. Interfaces 8 (2016) 22280.
[69] J. Li, M. Wang, G. Liu, L. Zhang, Y. He, X. Xing, Z. Qian, J. Zheng, C. Xu, Ind. Eng. Chem. Res. 57 (2018) 17401.
[70] D. Buzetzky, N.M. Nagy, J. Kónya, J. Radioanal. Nucl. Chem. 326 (2020) 1795.
[71] Y. Li, Z. Yang, K. Yang, J. Wei, Z. Li, C. Ma, X. Yang, T. Wang, G. Zeng, G. Yu, Sci. Total Environ. 821 (2022) 153174.
[72] W. Dou, X. Peng, L. Kong, X. Hu, Sci. Total Environ. 824 (2022) 153909.
[73] X. Peng, W. Dou, L. Kong, X. Hu, X. Wang, Environ. Sci. Tech. 53 (2018) 383.
[74] Y. Jiang, X. Zhang, L. Pei, S. Yue, L. Ma, L. Zhou, Z. Huang, Y. He, J. Gao, Chem. Eng. J. 339 (2018) 547.
[75] G.R. Berdiyorov, M.E. Madjet, K.A. Mahmoud, Membranes 11 (2021) 543.
[76] Y.A. Neolaka, Y. Lawa, J.N. Naat, A.A.P. Riwu, H. Darmokoesoemo, G. Supriyanto, C.I. Holdsworth, A.N. Amenaghawon, H.S. Kusuma, React. Funct. Polym. 147 (2020) 104451.
[77] W. Ma, X. Du, M. Liu, F. Gao, X. Ma, Y. Li, G. Guan, X. Hao, Chem. Eng. J. 412 (2021) 128576.
[78] S. Li, X. Dong, Y. Zhao, J. Mao, W. Chen, A. Chen, Y. Song, G. Li, Z. Jiang, W. Wei, Angew. Chem. Int. Ed. 61 (2022) e202210432.
[79] B. Kwak, S. Park, H.-S. Lee, J. Kim, B. Yoo, Front. Chem. 7 (2019) 637.
[80] P. Sarani, S. Sabbaghi, K. Rasouli, N.S. Mirbagheri, J. Rasouli, Inorg. Chem. Commun. 160 (2024) 111930.
[81] K.L. Gemene, M.E. Meyerhoff, Electroanalysis 24 (2012) 643.
[82] Y. Lee, H. Lee, D. Jung, Z. Chen, S. Lim, Materials 11 (2018) 560.